NEW SPECTROSCOPIC METHOD FOR THE OBSERVATION OF SEMICONDUCTOR INTERFACE STATES AND ITS APPLICATION TO MOS STRUCTURE*

H. Kobayashi, A. Asano, J. Ivanco, M. Takahashi
Institute of Scientific and Industrial Research, Osaka University, 8-1, Mihogaoka, Ibaraki, Osaka 567-0047, Japan

Y. Nishioka
Texas Instruments Tsukuba Research and Development Center Ltd., Miyukigaoka, Tsukuba, Ibaraki 305-0841, Japan

Received 26 June 2000, accepted 3 July 2000

We have developed a new method of observing energy distribution of interface states at ultrathin SiO_2/Si interfaces based on XPS measurement under bias. The analysis of the energy shift of the substrate Si 2p peak for the $\langle Pt/SiO_2/Si\rangle$ MOS structure vs. the bias voltage between Si and Pt provides the interface state spectra. We have also developed a new method of eliminating the interface states based on cyanide treatment. When the cyanide treatment is applied to solar cells with the $\langle ITO/SiO_2/Si(100)\rangle$ MOS structure, an energy conversion efficiency is increased to 16.2 % in spite of the simple cell structure.

PACS: 73.20.At, 84.60.Jt, 81.60.Cp, 79.60.Jv

1 Introduction

Interface states in the semiconductor band-gap play an important role in the determination of electrical characteristics of semiconductor devices such as metal- oxide-semiconductor (MOS) devices in LSI, solar cells, thin film transistors (TFT), chemical sensors, etc. Among the many kinds of interfaces, the Si/SiO_2 interface is the most widely used. With this interface, the interface state density is low (less than 1 % monolayer), but electrical characteristics are still strongly affected by it [1]. Because of the low state density, the energy distribution of the interface states cannot be obtained directly from conventional photoelectron spectroscopy measurements at zero bias.

In the present report, we introduce a new spectroscopic method for obtaining the energy distribution of low-density interface states. This is X-ray photoelectron spectroscopy (XPS) measurement under bias [2-6]. This method is applicable to a MOS structure with an ultrathin oxide layer for which interface state spectra cannot be obtained from electrical technique such as

*Presented at the Workshop on Solid State Surfaces and Interfaces II, Bratislava, Slovakia, June 20 – 22, 2000.

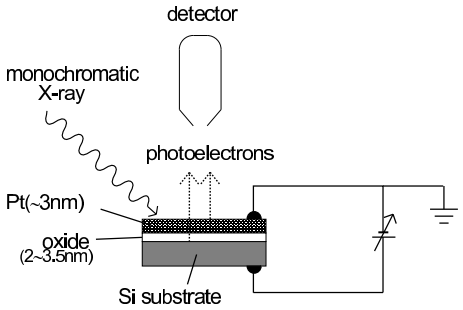

Fig. 1. Experimental set-up for XPS measurements under bias for obtaining interface state spectra.

capacitance-voltage (C-V) [7,8] or conductance-voltage (G-V) [9] measurements due to a tunneling current flowing through the ultrathin oxide layer. This method does not require assumptions such as equivalent circuits, uniform distribution of dopants, etc., which are usually involved in the electrical technique. Moreover, interface states in the whole band- gap region are observable as long as the interface Fermi level is shifted by biasing.

The interface states at Si/SiO_2 interfaces are usually eliminated by heat treatment at $350 \sim 450\ ^oC$ in hydrogen [10,11]. The hydrogen treatment forms Si-H bonds from Si dangling bonds [12]. However, Si-H bonds are ruptured above $\sim 550\ ^oC$ [13,14], and hence heat treatment cannot be performed after the hydrogen treatment. Moreover, irradiation such as by X-rays generates atomic hydrogen in the SiO_2 layer, and when it diffuses to the Si/SiO_2 interface, Si-H bonds are ruptured by the reaction with atomic hydrogen, resulting in the formation of Si dangling bond interface states [14-16]. In this report, we introduce a new method of eliminating interface states and defect states. This is the formation of Si-CN bonds from defect states by the use of cyanide treatment. This treatment improves the electrical characteristics of MOS devices.

2 Experimental

Phosphorus-doped n-type Si(100), Si(111) or polycrystalline wafers with a $\sim 10\ \Omega$cm resistivity were cleaned using the RCA method. In some cases, the wafers were immersed in a 0.1 M KCN aqueous solution for 2 min and rinsed in boiling water for 10 min. (Hereafter, this treatment is called "the cyanide treatment".) Then, a SiO_2 layer was formed by heat treatment in oxygen at temperatures ranging between 350 and 700^oC. For measurements of XPS spectra under bias to obtain interface state spectra, a ~ 3 nm thick platinum (Pt) film was deposited on the SiO_2 layer while for measurements of solar cell and conductance-voltage (G-V) characteristics, indium thin oxide (ITO) and aluminum (Al) films were deposited, respectively.

XPS spectra were recorded using a VG SCIENTIFIC ESCALAB 220i-XL spectrometer with a monochromatic Al Kα radiation source. During XPS measurements, the Pt layer was connected to the ground and a bias voltage was applied to the Si substrate, as shown in Fig. 1. The electron pass energy in the hemispherical analyzer was set at 10 eV and photoelectrons were collected in the surface-normal direction.

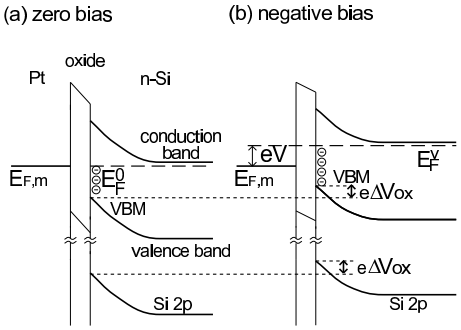

Fig. 2. Band diagrams of n-type Si-based MOS structure: (a) at zero bias; (b) under a negative bias, V, applied to the Si with respect to the metal.

Solar cell characteristics were measured under Air Mass (AM) 1.5 100 mWcm^{-2} irradiation. G-V measurements were performed at 1 MHz using a YHP 4192A impedance analyzer.

3 Theoretical basis

Figure 2 shows the band diagrams of a n-type Si-based MOS structure. (The following discussion could be valid for a p-type Si-based MOS structure.) Due to the difference between the interface state neutral level and the bulk Si Fermi level, electrons in the Si-bulk transfer to interface states, forming the space charge layer in Si, and consequently the Si band bends upward. Due to the difference between the interface state neutral level and the metal Fermi level, electron transfer occurs between the metal and the interface states, which causes a potential drop across the oxide layer. Since the width of the space charge layer for the devices used in the present study (donor density: $\sim 5 \times 10^{14}$ cm^{-3}) is ~ 0.5 μm (much wider than the photoelectron mean free path of ~ 3 nm), the potential in the photoelectron detected Si region can be considered to be constant.

At zero bias, the metal Fermi level, $E_{F,m}$, and the Si Fermi level, E_F^0, are located at the same energy. In this case, interface states below E_F^0 are empty while those above E_F^0 are occupied by electrons. By the application of a negative (or positive) bias, V, to the Si with respect to the metal, the Si Fermi level, E_F^V, is shifted upward (or downward) by the magnitude of eV (energy reference: Si valence band maximum). Consequently, interface states with energies between E_F^V and E_F^0 are newly occupied (or vacated) by electrons. This interface state charge, Q_{it}, induced by the bias is given by the integration of the interface state density, D_{it}, with respect to the energy between E_F^0 and E_F^V:

$$Q_{it} = e \int_{E_F^0}^{E_F^V} D_{it}(E) dE. \tag{1}$$

This interface state charge, Q_{it}, induces a change in the potential drop across the oxide layer with a magnitude given by

$$\Delta V_{ox} = Q_{it}/C_{ox} = e \int_{E_F^0}^{E_F^V} D_{it}(E) dE/C_{ox}, \tag{2}$$

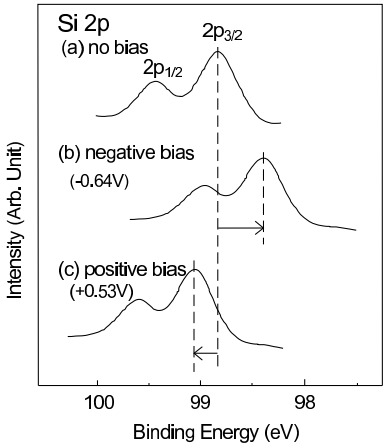

Fig. 3. XPS spectra in the Si 2p region for the $\langle Pt/SiO_2/Si(111)\rangle$ MOS structure: (a) at zero bias; (b) at -0.64 V; (c) at 0.53 V.

where C_{ox} is the oxide capacitance which is given by

$$C_{ox} = \epsilon_{ox}/d, \tag{3}$$

where ϵ_{ox} is the permittivity of the oxide layer and d is the oxide thickness. Since the energy between $E_{F,m}$ and the oxide band at the metal/oxide interface and that between the oxide band and the Si core level (e.g., Si 2p level) at the oxide/Si interface are constant, the semiconductor core level is shifted by a magnitude which is the same as the change in the potential drop across the oxide layer, ΔV_{ox}.

On the other hand, the interface Fermi level under bias, E_F^V, with respect to the Si valence band maximum is written by

$$E_F^V = E_F^0 + eV - e\Delta V_{ox}, \tag{4}$$

where V is defined as positive (or negative) for a negative bias (or positive bias) applied to the semiconductor and ΔV_{ox} is defined as positive for the upward band- edge shift. Eq. (4) means that the net bias across the Si space charge layer is reduced to $V - \Delta V_{ox}$ due to the presence of the interface states.

ΔV_{ox} is also induced by a change in the depletion layer charge, but its magnitude is estimated to be less than ten millivolts, negligible when compared with that induced in the interface state charge, and thus this shift is neglected in the present analysis.

In the present study, the shift of the substrate Si 2p level (i.e., ΔV_{ox}) is observed as a function of bias voltage, V, and $D_{it}(E)$ is obtained as a function of energy, E, using Eqs. (2) and (4).

4 Results and discussion

Figure 3 shows the example of the Si 2p XPS spectra for the $\langle Pt/SiO_2/n\text{- }Si(111)\rangle$ MOS structure. Doublet peaks are due to the Si $2p_{3/2}$ and $2p_{1/2}$ levels of the substrate. A broad peak due to the

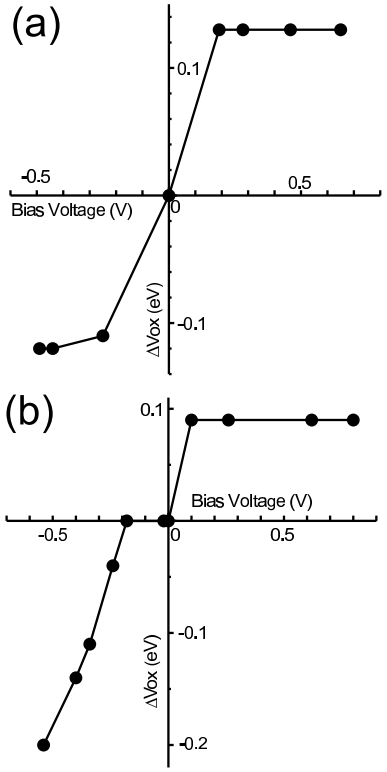

Fig. 4. Plots of the energy shift of the substrate Si 2p peak for the $\langle Pt/SiO_2/Si(111)\rangle$ MOS structure vs. the bias voltage applied between Pt and Si. The SiO_2 layers were formed by heating in oxygen at the following temperatures: (a) 350 ^{o}C; b) 700 ^{o}C.

SiO_2 layer was present in the higher energy region (not shown in the figure). Based on the ratio in the area intensities between these peaks, the oxide thickness is estimated to be 2.5 nm.

By the application of a negative bias voltage to the Si with respect to the Pt overlayer, the substrate Si 2p peak was shifted toward a lower binding energy [spectrum (b)], while by the application of a positive bias voltage, it was shifted in the higher energy direction [spectrum (c)]. These shifts disappeared completely with the removal of the bias voltage, and thus they were attributable to charges accumulated in interface states.

Figure 4 shows the plots of the energy shifts of the substrate Si 2p peak vs. the bias voltage for the $\langle$Pt/ultrathin thermal $SiO_2/Si(111)\rangle$ MOS structure. For both the devices investigated, the shifts were positive (or negative) in the reverse (forward) bias region. However, the character of the plots strongly depended on the oxide formation temperature, indicating the difference in the energy distribution of interface states. It should be noted that there are several bias regions where the energy shift completely stops. These regions correspond to the energy regimes without interface states.

Figure 5 shows the energy distribution of interface states obtained from the analysis of Fig. 4 using Eqs. (2) and (4). Both the interface state spectra have a peaked-structure. This result shows

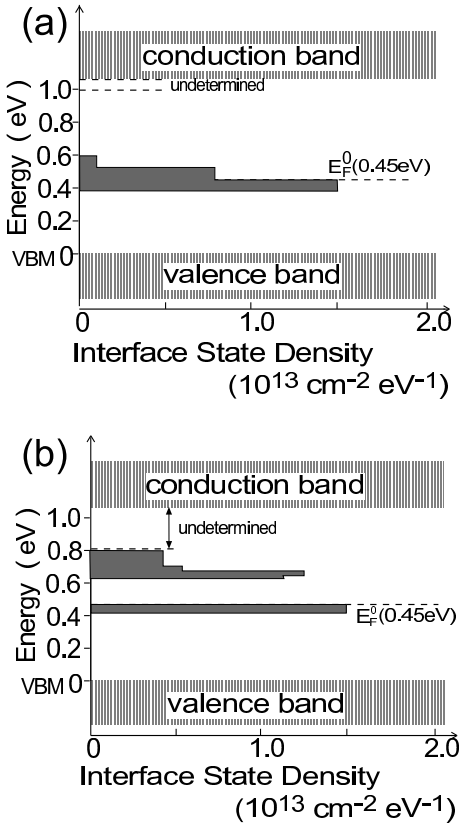

Fig. 5. Interface state spectra obtained from the analysis of Fig. 4 for the $\langle Pt/SiO_2/Si(111)\rangle$ MOS structure with the ultrathin thermal SiO_2 layers formed at the following temperatures: a) 350 ^{o}C; b) 700 ^{o}C.

that the interface states are due to defect states such as Si dangling bonds at the interface [17,18], but not caused by the fluctuation of bond angles and bond lengths near the interface which causes U-shaped interface state spectra [19]. For the SiO_2 layer formed at 350 ^{o}C, one interface state peak is present near the midgap. For the SiO_2 layer formed at 700 ^{o}C, on the other hand, two interface state peaks are present, one above and the other below the midgap. To clarify the origin of the interface state peaks, theoretical calculations were performed as described below.

Figure 6 shows cluster models employed in the calculations of the interface state energy level using a density functional theory (DFT) method. The central Si atom has a dangling bond pointing in the interface-normal direction and other interface Si atoms are bound to three Si atoms and one oxygen atom, simulating the $Si(111)/SiO_2$ interface. The calculations show that an isolated Si dangling bond at the interface [Fig. 6(a)] has an energy level near the midgap. For an anion cluster formed by the addition of an electron to the cluster of Fig. 6(a), the interface state level is calculated to be located at $\sim$ 0.1 eV above that of the neutral cluster. This result shows that the effective correlation energy of Si dangling bonds has such a small positive value. The calculations can well explain the interface state spectrum for the 350 ^{o}C-thermal oxide layer.

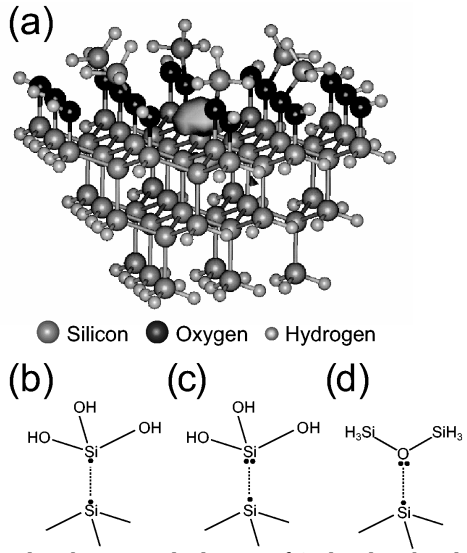

Fig. 6. Cluster models employed in the DFT calculations of Si dangling bond energy: (a) for an isolated Si dangling bond; (b) for a Si dangling bond interacting weakly with a Si atom having an unpaired electron; (c) for a Si dangling bond interacting weakly with a Si atom having lone-pair electrons; (d) for a Si dangling bond interacting weakly with an oxygen atom having lone-pair electrons.

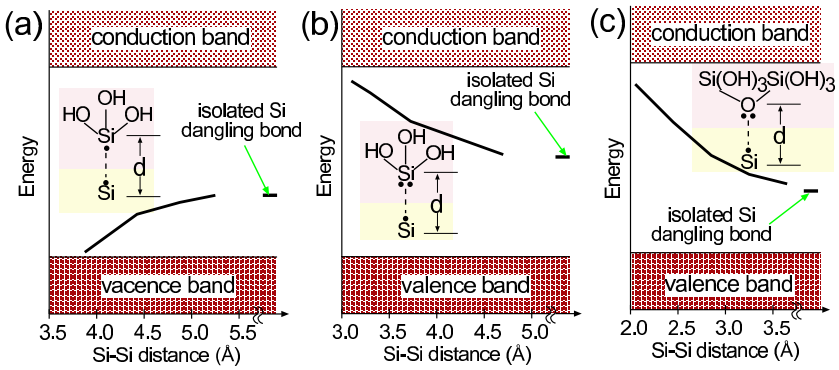

Fig. 7. Calculated energy level of a Si dangling bond under the following environments: (a) with a weakly interacting Si atom having an unpaired electron; (b) with a weakly interacting Si atom having lone-pair electrons; (c) with a weakly interacting oxygen atom having lone-pair electrons. The Si dangling bond energy is calculated as a function of the distance between the dangling bond Si atom and the interacting atom.

The peak near the midgap is due to isolated Si dangling bonds and because of the small correlation energy, two transitions, [(0/+) and (-/0)], are included in this one peak. Therefore, the well-separated peaks for the 700 ^{o}C-thermal oxide layer are not attributable to different transitions of one kind of interface state but due to different kinds of interface states.

In the cluster model of Fig. 6(b), a Si atom with an unpaired electron is located near the Si

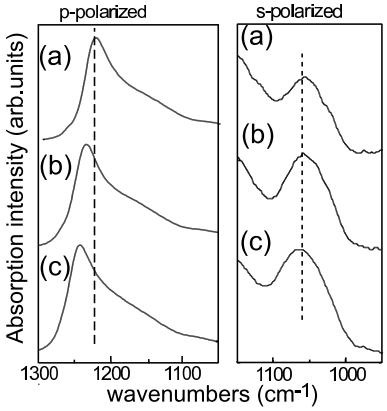

Fig. 8. FT-IR-ATR spectra for the SiO_2 layers formed by the heat treatment of Si(111) in oxygen at the following temperatures: (a) 350 ^{o}C; (b) 550 ^{o}C; (c) 700^{o}C.

dangling bond and interacts weakly. (The structure only near the Si dangling bond is shown in the figure and the rest of the cluster is the same as that of Fig. 6(a)). Calculations show that the Si dangling bond energy shifts toward the valence band as the distance between these Si atoms becomes shorter, as shown in Fig. 7(a). In the model of Fig. 6(c) [or Fig. 6(d)], on the other hand, a Si (or oxygen) atom with lone-pair electrons is located close to the Si dangling bond. In this case, the Si dangling bond energy shifts toward the conduction band as shown in Figs. 7(b) and (c). Therefore, the interface state peaks for the 700 ^{o}C-thermal SiO_2 layer [Fig. 5(b)] are attributable to Si dangling bonds with which a Si or oxygen atom in the SiO_2 layer interacts weakly. The dependence of the interface state energy on the oxidation temperature is attributable to a change in the atomic density of the SiO_2 layer, as explained below.

Figure 8 shows the FT-IR-ATR spectra for the thermal SiO_2 layers. The vibrational frequency of LO phonons of the asymmetric Si-O vibration, ν_{LO}, became higher as the oxidation temperature was increased. The vibrational frequency of the TO phonons, ν_{TO}, on the other hand, was only slightly affected by the oxidation temperature (i.e., 1057 cm^{-1} for the 350 ^{o}C-thermal SiO_2 layer and 1065 cm^{-1} for the 700 ^{o}C-thermal SiO_2 layer). The relation between ν_{LO} and ν_{TO} is given by [20,21]

$$\nu_{LO}^2 - \nu_{TO}^2 = \frac{C_2\rho}{1 + C_1\rho} \tag{5}$$

where ρ is the atomic density of the SiO_2 layer, C_2 is a constant related to the dynamical charge for the Si-O vibration, and C_1 is given by

$$C_1 = \frac{\epsilon - 1}{\rho} \tag{6}$$

where ϵ is the relative dielectric constant of the SiO_2 layer. Using the values for a thick thermal SiO_2 layer (i.e., $\nu_{LO} = 1070$ cm^{-1}, $\nu_{TO} = 1255$ cm^{-1}, and $\rho = 2.28 \times 10^{22}$ cm^{-3}), C_1 and C_2 are determined. Using these values, the atomic density, ρ, for the thermal SiO_2 layers formed at 350, 550, and 700 ^{o}C are estimated to be 1.57×10^{22}, 1.84×10^{22}, and 1.93×10^{22} cm^{-3}, respectively, meaning that the higher the oxidation temperature, the higher the atomic density of

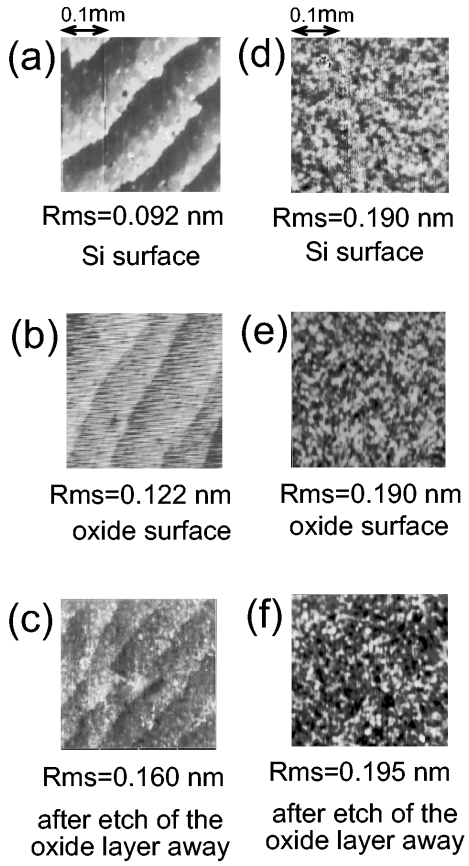

Fig. 9. AFM images for the following Si(111) surfaces: (a) atomically flat surface before oxidation; (b) atomically flat surface after chemical oxidation using HNO_3; (c) atomically flat surface after etching the SiO_2 layer away; (d) atomically rough surface before oxidation; (e) atomically rough surface after chemical oxidation using HNO_3; (f) atomically rough surface after etching the SiO_2 layer away.

the SiO_2 layer. When the atomic density is low, the SiO_2 layer has a soft structure which can be changed by the presence of substrate Si atoms near the SiO_2 atoms. Consequently, the distance between a Si dangling bond atom and an atom in the SiO_2 layer becomes large, resulting in an isolated Si dangling bond which possesses an energy level near the midgap [Fig. 5(a)]. The high-density SiO_2 layers, on the other hand, have a hard structure which cannot be changed by nearby substrate Si atoms. Consequently, a Si or oxygen atom in the SiO_2 layer is present near a Si dangling bond atom at the interface, and interacts weakly. The weak interaction shifts the Si dangling bond energy level upward or downward from the midgap, depending on whether the interacting atom has lone-pair electrons or an unpaired electron.

In the case of a Si(111) substrate, atomically flat surfaces can be produced easily by etching with NH_4F [24]. With the atomically flat surfaces, bilayer steps were clearly seen [Fig. 9(a)]. Such bilayer steps were not observed for the atomically rough Si surfaces [Fig. 9(d)].

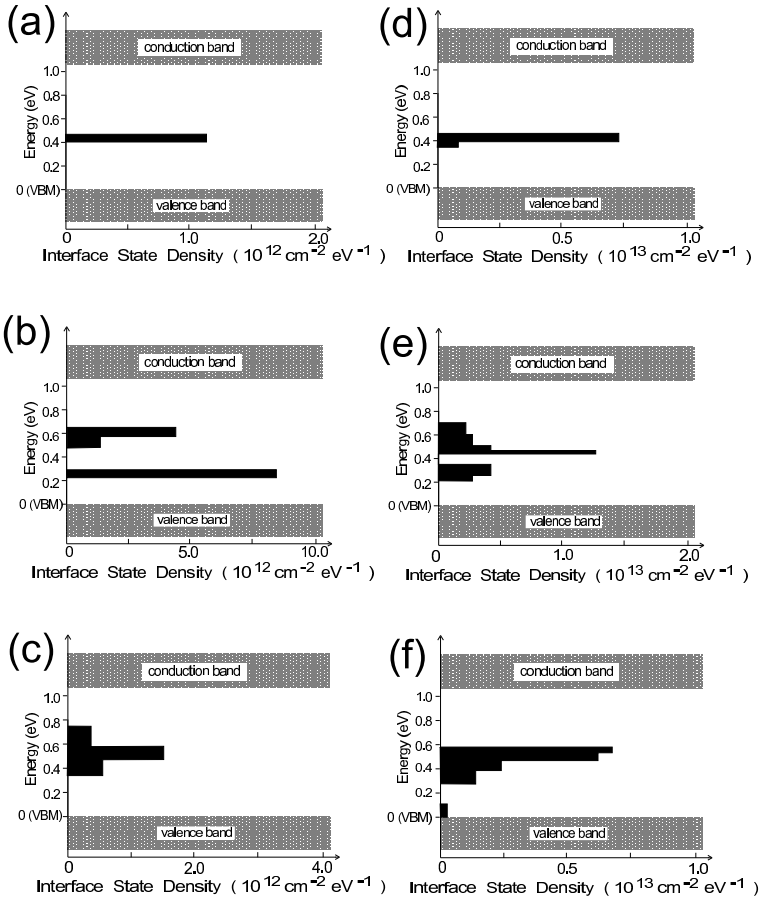

Fig. 10. Interface state spectra for the ⟨Pt/SiO_2/Si(111)⟩ MOS structure with the ultrathin chemical SiO_2 layer formed with the following solutions: (a) and (d) HCl+H_2O_2.; (b) and (e) HNO_3; (c) and (f) H_2SO_4+H_2O_2. Spectra (a), (b) and (c) are for atomically smooth interfaces, while spectra (d), (e), and (f) are for atomically rough interfaces.

When the atomically flat Si surfaces were oxidized by the immersion in HCl+H_2O_2, HNO_3, or H_2SO_4+H_2O_2, bilayer steps were still observed [Fig. 9(b)]. Bilayer steps were also observed after the SiO_2 layer was etched away [Fig. 9(c)], indicating that Si/SiO_2 interfaces formed from atomically flat surfaces were atomically smooth. On the other hand, Si/SiO_2 interfaces were rough [Fig. 9(f)] when rough surfaces were oxidized.

Figure 10 compares the interface state spectra for atomically smooth [spectra (a) and (c)] and rough [spectra (d) and (f)] interfaces. The energy distribution depended on the oxide formation method, i.e., one sharp peak for the HCl+H_2O_2 oxide [spectra (a) and (d)], two peaks for the HNO_3 oxide [spectra (b) and (e)], and one broad peak for the H_2SO_4+H_2O_2 oxide [spectra (c) and (f)], but they did not greatly depend on the roughness at the interfaces. FT-IR-ATR measurements showed that the SiO_2 layer formed in HCl+H_2O_2 had a lower atomic density than

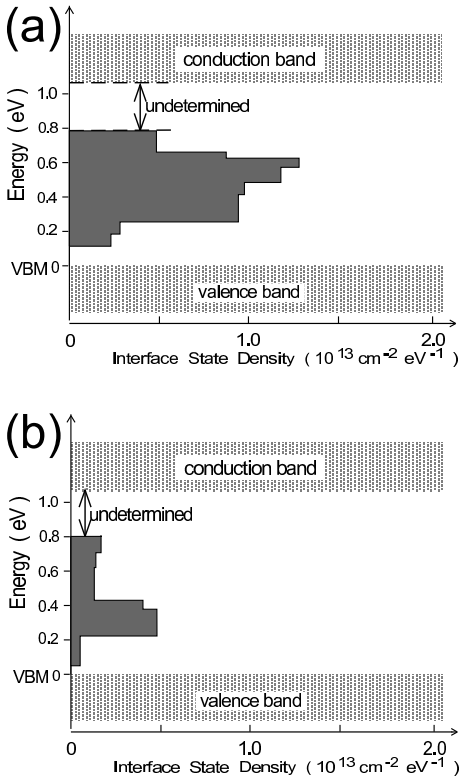

Fig. 11. Interface state spectra for the $\langle Pt/SiO_2/Si(100)\rangle$ MOS structure with the ultrathin SiO_2 layer formed by heat treatment at 450 ^oC in oxygen: (a) without cyanide treatment; (b) with cyanide treatment.

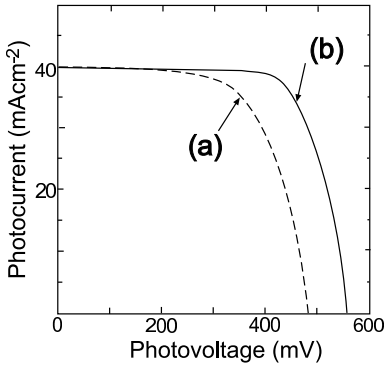

Fig. 12. Photovoltage-photocurrent curves for $\langle$ITO/ultrathin SiO_2/mat-textured Si(100)$\rangle$ MOS solar cells: (a) without cyanide treatment; (b) with cyanide treatment.

those for the oxide layers formed in HNO_3 and H_2SO_4+H_2O_2 [24]. On the other hand, the interface state density depended greatly on the interfacial roughness. We think that steps hinder

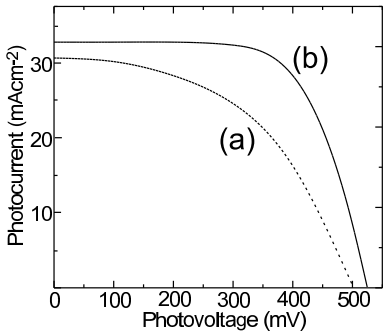

Fig. 13. Photovoltage-photocurrent curves for ⟨ITO/ultrathin SiO_2/poly-Si⟩ MOS solar cells: (a) without cyanide treatment; (b) with cyanide treatment.

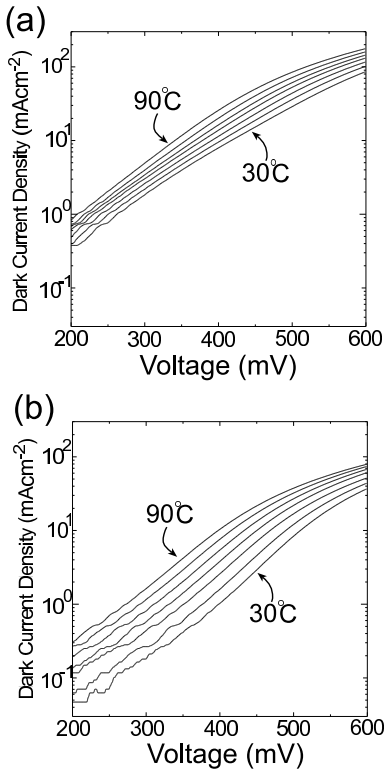

Fig. 14. Dark current-voltage curves for ⟨ITO/ultrathin SiO_2/poly-Si⟩ MOS solar cells measured at various temperatures: (a) without cyanide treatment; (b) with cyanide treatment.

the formation of complete SiO_2 network, resulting in Si dangling bond interface states near the step edges.

We have developed a simple new method to eliminate interface states at Si/SiO_2 interfaces. This is the cyanide method in which Si is immersed in a KCN solution followed by a rinse in

water [25,26]. Figure 11 shows interface state spectra for the ⟨Pt/450 ^{o}C-thermal SiO_2/Si(100)⟩ MOS structure without [spectrum (a)] and with [spectrum (b)] cyanide treatment. The interface state density was decreased to $\sim 1/5$ by the cyanide treatment. Theoretical calculations using the DFT method show that the gap-state disappears with the formation of a Si-CN bond from a Si dangling bond. Calculations also show that a CN^- ion is bound to a dangling bond Si atom via the carbon atom and the Si-CN bond has a linear structure. The Si-CN bond energy is calculated to be ~ 4 eV, much higher than the Si-H bond energy of 2.6 eV [27]. Due to the high bond energy, Si-CN bonds are much more stable than Si-H bonds.

Figure 12 shows the photocurrent-photovoltage ($I_{ph} - V_{ph}$) curves for the ⟨ITO/SiO_2/Si(100)⟩ MOS structure. The thickness of the SiO_2 layer was less than 1.5 nm to allow a photocurrent to tunnel easily [28]. Before the oxide formation, mat-textured Si surfaces with pyramidal structures [29] were produced by alkali etching in order to decrease the surface reflectivity. Consequently, a high photocurrent density of ~ 40 mAcm^{-2} (theoretical limit: 45 mAcm^{-2}) under AM 1.5 100 mWcm^{-2} irradiation was achieved. Therefore, for a further increase in the conversion efficiency, an increase in photovoltage is necessary, and this was achieved by the cyanide treatment. The increase in the photovoltage due to the cyanide treatment was ~ 80 mV. The open circuit photovoltage, V_{OC}, is given by [30]

$$V_{OC} = \frac{nkT}{e} \ln \left(\frac{I_{ph}}{I^0_{dark}} + 1 \right), \tag{7}$$

where n is the ideality factor, I_{ph} is the photocurrent density, and I^0_{dark} is the dark saturation current denstity. From Eq. (7), I^0_{dark} is calculated to have decreased to $\sim 1/10$ for an increase in the photovoltage of 80 mV. This vast decrease in I^0_{dark} is achieved by the elimination of interface states that causes the following two effects: i) a decrease in the density of a majority carrier thermionic emission dark current resulted from the enhancement in Si band-bending due to the unpinning of the interface Fermi level, and ii) a decrease in the interface recombination dark current density.

When the cyanide treatment was performed on polycrystalline Si, a greater improvement was achieved. Figure 13 shows the $I_{ph} - V_{ph}$ curves for the polycrystalline Si-based solar cells with the ⟨ITO/SiO_2/poly-Si⟩ structure. In this case, not only the open-circuit photovoltage but also the short-circuit photocurrent density and fill factor are improved, and consequently a conversion efficiency of 12.5 % was achieved (~ 50 % increase) in spite of the simple cell structure with polycrystalline Si.

Figure 14 shows the dark current-voltage (I-V) curves for the ⟨ITO/SiO_2/poly- Si⟩ MOS structure. Without cyanide treatment, the dark current density depended only slightly on the temperature [Fig. 14(a)]. With the cyanide treatment, on the other hand, the dark current density became strongly dependent on the temperature, and it decreased by more than one order of magnitude [Fig. 14(b)]. From a detailed analysis of Fig. 14, the dark current flow mechanisms can be elucidated. Without cyanide treatment, high-density defect states are present in the polycrystalline Si. Electrons in the Si bulk flow to the Si surface by hopping the defect states in the depletion layer [Fig. 15(a)] (trap-assisted multistep tunneling [31]). Due to the tunneling mechanism, the dark current density was only weakly dependent on the temperature. The defect states in the Si depletion layer are eliminated by the cyanide treatment, and consequently thermal excitation becomes necessary for the electron flow [Fig. 15(b)]. Due to thermal excitation, the dark current density became strongly dependent on the temperature and became markedly lower.

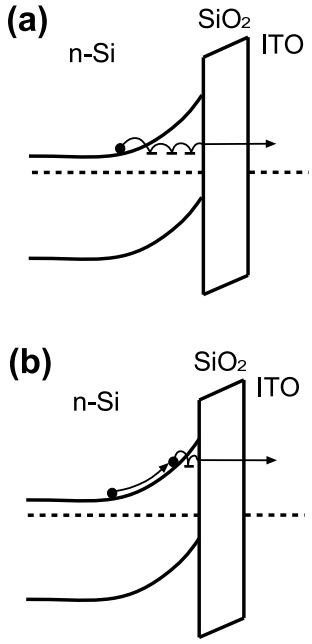

Fig. 15. Dark current flow mechanisms for ⟨ITO/ultrathin SiO_2/poly-Si⟩ MOS solar cells: (a) without cyanide treatment; (b) with cyanide treatment.

5 Conclusion

We have developed a new method of observing interface state spectra based on XPS measurements under bias. The analysis of the bias-induced energy shift of the substrate Si 2p peak measured as a function of the bias voltage provides the energy distribution of interface states. This method can be applied to ultrathin oxide layers for which interface states cannot be obtained using the electrical technique. Assumptions such as equivalent circuits are not necessary for this method. Using this excellent method, interface state spectra for ultrathin SiO_2/Si interfaces are obtained. The interface state spectra have peaked-structure and the peaks are attributable to Si dangling bonds at the interface. The interface state energy greatly depends on the atomic density of the SiO_2 layer. For low atomic density SiO_2 layers, e.g., SiO_2 layers formed at low temperatures, an interface state peak is observed near the midgap and it is attributable to isolated Si dangling bonds. For high atomic density SiO_2 layers, on the other hand, two interface state peaks are observed, one above and the other below the midgap, and they are attributable to Si dangling bonds interacting weakly with a Si or oxygen atom in the SiO_2 layer. The interface state density strongly depends on the interfacial roughness. The interface state density is decreased markedly by the cyanide method in which Si is simply immersed in KCN solutions followed by a rinse in water. When the cyanide treatment is performed on ⟨ITO/SiO_2/mat-textured Si(100)⟩ MOS solar cells, the photovoltage is increased by $\sim$ 80 mV and a conversion efficiency of 16.2 % is achieved. When the cyanide treatment is applied to ⟨ITO/SiO_2/poly-Si⟩ MOS solar cells, defect states in polycrystalline Si are eliminated, leading to a change in the dark current flow

mechanism from trap-assisted multistep tunneling to thermionic emission, and a vast increase as much as 12.5 % in the conversion efficiency is achieved.

References

[1] E. H. Nicollian and J. R. Brews: *MOS (Metal Oxide Semiconductor) Physics and Technology*, Wiley, New York, 1982

[2] Y. Yamashita, A. Asano, Y. Nishioka, and H. Kobayashi: *Phys. Rev. B* **59** (1999) 15872

[3] H. Kobayashi, K. Namba, Y. Yamashita, Y. Nakato, T. Komeda, and Y. Nishioka: *J. Appl. Phys.* **80** (1996) 1578

[4] H. Kobayashi, Y. Yamashita, Y. Nakato, T. Komeda, and Y. Nishioka: *Appl. Phys. Lett.* **69** (1996) 2276

[5] Y. Yamashita, K. Namba, Y. Nakato, Y. Nishioka, and H. Kobayashi: *J. Appl. Phys.* **79** (1996) 7051

[6] H. Kobayashi, K. Namba, T. Mori, and Y. Nakato: *Phys. Rev. B* **52** (1995) 5781

[7] C. N. Berglund: *IEEE Trans. Electron Devices* **ED-13** (1966) 701

[8] L. M. Terman: *Solid-State Electron.* **5** (1962) 285

[9] E. H. Nicollian and A. Goetzberger: *Bell Syst. Tech. J.* **46** (1967) 1055

[10] M. L. Reed and J. D. Plummer: *J. Appl. Phys.* **63** (1988) 5776

[11] T. W. Hickmott: *J. Appl. Phys.* **48** (1977) 723

[12] E. H. Poindexter and P. J. Caplan: *Prog. Surf. Sci.* **14** (1983) 201

[13] P. J. Caplan, E. H. Poindexter, B. E. Deal, and R. R. Razouk: *J. Appl. Phys.* **50** (1979) 5847

[14] F. B. McLean: *IEEE Trans. Nucl. Sci.* **NS-27** (1980) 1651

[15] D. L. Griscom: *J. Electron. Mater.* **21** (1992) 763

[16] E. F. da Silva, Jr., Y. Nishioka, and T.-P. Ma: *Appl. Phys. Lett.* **51** (1987) 270

[17] R. B. Laughlin, J. D. Joannopoulos, and D. J. Chadi: *Phys. Rev. B* **21** (1980) 5733

[18] T. Sakurai and T. Sugano: *J. Appl. Phys.* **52** (1981) 2889

[19] R. B. Laughlin, J. D. Joannopoulos, and D. J. Chadi: in *The Physics of SiO_2 and Its Interfaces*, ed. S. T. Pantelides, Pergamon, New York, 1978, Chap.6

[20] A. Lehmann, L. Schumann, and K. Hbner: *Phys. Status Solidi B* **117** (1983) 689

[21] R. A. B. Devine: *Appl. Phys. Lett.* **68** (1996) 3108

[22] Y. Sugita, S. Watanabe, N. Awaji, and S. Komiya: *Appl. Surf. Sci.* **100/101** (1996) 268

[23] G. S. Higashi, R. S. Becker, Y. J. Chabal, and A. J. Becker: *Appl. Phys. Lett.* **58** (1991) 1656

[24] Y. Yamashita, A. Asano, Y. Nishioka, and H. Kobayashi: *Phys. Rev. B* **59** (1999) 15872

[25] H. Kobayashi, S. Tachibana, K. Yamanaka, Y. Nakato, and K. Yoneda: *J. Appl. Phys.* **81** (1997) 7630

[26] H. Kobayashi, A. Asano, S. Asada, T. Kubota, Y. Yamashita, K. Yoneda, and Y. Todokoro: *J. Appl. Phys.* **83** (1998) 2098

[27] K. L. Brower and S. M. Myers: *Appl. Phys. Lett.* **57** (1990) 162

[28] H. C. Card: *Solid-State Electron.* **20** (1977) 971

[29] H. Kobayashi. Y. Kogetsu, T. Ishida, and Y. Nakato: *J. Appl. Phys.* **74** (1993) 4756

[30] S. M. Sze: *Physics of Semiconductor Devices*, 2nd ed.,Wiley, New York, 1981

[31] A. R. Riben and D. L. Feucht: *Int. J. Electron.* **20** (1966) 583